Structures 16 (2018) 390–404

Contents lists available at ScienceDirect

Structures

journal homepage: www.elsevier.com/locate/structures

Experimental evaluation of rigid connection with reduced section and replaceable fuse

AllahReza Moradi Garoosi[a], Mehrzad TahamouliRoudsari[a,*], Behrokh Hosseini Hashemi[b]

[a] Department of Civil Engineering, Kermanshah Branch, Islamic Azad University, Kermanshah, Iran
[b] Structural Eng. Research Center, The International Institute of Earthquake Engineering and Seismology (IIEES), Tehran, Iran

ARTICLE INFO

Keywords:
Steel moment resisting frame
Rigid connection
Replaceable fuse
Beam with reduced flange section
Beam with reduced depth section

ABSTRACT

The reduced Beam Section (RBS) connection was proposed after the 1994 Northridge earthquake. By creating a plastic hinge outside the connection area, this connection minimizes the damage inflicted upon the panel zone. But, after the occurrence of a medium-intensity earthquake, the entire beam would have to be replaced due to the concentration of damage in the reduced area, which is practically impossible. This study aims to experimentally investigate the use of the reduced section in a replaceable fuse. Thus, four rigid connections including an Ordinary end-plate Bolted Connection (OBC), an ordinary RBS connection (RBS), a fuse including an RBS connection (RBS−F), and a Reduced Depth Section (RDS-F) connection incorporating a fuse were evaluated. The static cyclic load was applied and the moment-drift hysteresis diagram was plotted. The properties of the column and the panel zone were selected so that damage would be sustained by the beam and the performance of the four connections could be compared. Even though all of the samples satisfied the drift criteria of the rigid connection in the special moment resisting frame, the amount of rotation in the panel zone of the OBC sample was 2 to 3 times greater than the other three samples. Therefore, using different types of RBS connections reduces the damage inflicted upon the column and the panel zone. The results show that in addition to having very good ductilities and the ability to be replaced after earthquakes, the RBS-F and RDS-F samples can be suitable replacements for the ordinary RBS connections.

1. Introduction

In accordance with the recommendation of different design codes, using intermediate and special moment resisting frames in regions with high seismic risk is of utmost importance. In the 1994 Northridge earthquake, considerable damage was inflicted on the beam-column connection area of moment resisting frames. Up until that time, it was believed that rigid connections with complete penetrating groove weld can withstand high levels of plastic deformation. However, the developed cracks and the brittle failures in the connections revealed that the actual ductility in these connections might be lower than the prediction design codes put forth.

To improve the performance of rigid connections in special moment resisting frames subjected to strong seismic excitation, two solutions were suggested: strengthening the connection or weakening the beam in the vicinity of the connection. The second approach, which is known as the RBS connection, causes plastic hinge to take form outside the connection, while at the same time reducing the force and moment existing within the connection. The RBS was one of the prequalified connections that were approved by the AISC [1] after the 1994 Northridge earthquake. Another prequalified rigid connection is the end-plate bolted connection with stiffener. Simultaneous use of end-plates and the RBS can improve the performance of the connection. In this connection, in addition to the fact that the weld connecting the beam to the end-plates was carried out in the factory, the use of the reduced cross-section has expelled damage concentration out of the connection. The only problem with this connection is that damage concentration occurs within the reduced area and after average or strong earthquakes, the entire beam would need to be replaced which is almost impossible.

Tremblay et al. investigated the performance of steel structures during the Northridge and Kobe earthquakes [2,3]. The brittle failure and the damage inflicted upon the connections in moment resisting frames showed that the design criteria in practice prior to the 1994 Northridge earthquake did not guarantee the formation of plastic hinge in the beam. They suggested that the pre-Northridge connections, even if they had sustained a small degree of damage, should be closely re-evaluated after the earthquake. Numerous numerical and experimental

* Corresponding author.
E-mail address: tahamouli@iauksh.ac.ir (M. TahamouliRoudsari).

https://doi.org/10.1016/j.istruc.2018.11.010
Received 2 March 2018; Received in revised form 26 October 2018; Accepted 11 November 2018
Available online 12 November 2018

studies were carried out on RBS connections subjected to seismic loads to form a good understanding of their behavior. Among those studies, the work carried out by Zhang and Ricles [4] can be mentioned, wherein the authors experimentally evaluated RBS beam-deep column connections. By investigating six samples, they showed that deep columns laterally anchored by ceiling slabs can increase the strength of the RBS connection. Wilkinson et al. [5] evaluated a type of RBS connection by decreasing the height of the beam's web. The model they recommended had a decreased web height that resembled a wedge. This sample had a somewhat suitable performance, although in the hysteresis diagram, the pinching effect was quite evident. Han et al. [6] put forth new design equations for determining the bending strength of a bolted web RBS connections. They showed that compared to the criteria given by FEMA 350, these design equations have good accuracy and guarantee the formation of the plastic hinge in the reduced zone. Hedayat and Celikag [7] conducted a numerical study on Post-Northridge connections with web openings. The assessments showed that in addition to transferring the location of the plastic hinge away from the connection, controlling the reduced area of the web with different geometrical shapes can increase the ductility and improve the seismic performance of the moment resisting frame.

Pachoumis et al. [8] performed experimental and numerical evaluations on beams with reduced sections subjected to cyclic loads. Two identical experimental samples were constructed, with the only difference being in the depth of the reduced area. The results showed that the sample with a larger depth reduction had a more suitable behavior. Mirghaderi et al. [9], performed some tests to investigate the seismic behavior of RBS connections with accordion webs. Using the obtained experimental and numerical results, they showed that using the accordion web in the beam causes no noticeable strength reduction in the structure and increases ductility in the hysteresis loops. Design and seismic performance of steel moment resisting frames incorporating replaceable fuses was studied and evaluated by Shen et al. [10]. The results indicate that steel moment resisting frames with replaceable links possess a suitable ductility, with the added coup that the link can be replaced after earthquake. Mashaly et al. [11] assessed the behavior of the four-screw extended end-plate connection subjected to lateral load. The connection reached a rotation of 0.05 Rad which signifies the ductile behavior of the connection. The researchers also showed that the extended end-plate brings about a higher energy dissipation.

Chi et al. [12] conducted research on the seismic behavior of concrete-filled square tubular column connections with reduced beam section subjected to cyclic loading. The results showed that the location where the plastic hinge formed was driven towards the reduced region of the beam and this type of connection possesses adequate ductility and a suitable ability for energy dissipation. Using ANSYS, a numerical study was carried out by Maleki and Tabbakhha [13] on the beam with slotted–Web–reduced–flange rigid moment connection. The proposed model had a better performance compared to other samples. Ghassemieh and Kiani [14] seismically evaluated frames with reduced beam sections by taking into account the flexibility of the connection. Numerical analyses of a structure under the influence of far field and near field earthquakes revealed that without considering the flexibility of beam–column connections, the result of the analysis might not be reliable.

The influence of gravity loads on the seismic design of RBS connections was investigated by Montuori [15]. In this study, to ensure the formation of the plastic hinge in the reduced area, a new relationship was proposed to assess the correlation between gravity load, the RBS area, and the level of section reduction. In an experimental and numerical study, Sofias et al. [16] investigated the RBS-end plate rigid connection subjected to cyclic load. They showed that the flexural beam-column connection in the location of the end-plate remains in the elastic state and no damage is inflicted upon the end-plate and the components of the connection, and that damage is concentrated in the reduced section area. Swati and Gaurang [17], in an experimental and numerical study, investigated beams with/without reduced sections. By calibrating the ANSYS software based on the experimental and numerical results, it was shown that the RBS sample displays a suitable performance.

Table 1
Dimensions of the column and the beam.

	Flange (mm)	Web (mm)
Beam	180 × 15	150 × 8
Column	240 × 20	200 × 10

Abdollahzadeh et al. [18] determined the hysteresis behavior of end-plate bolted beam – column rigid connections using mechanical models and Artificial Neural Networks. It was concluded that the mechanical model does not incorporate all the aspects of the hysteresis response and is not adequately accurate compared to the model constructed based on Artificial Neural Networks. Roudsari et al. [19] carried out numerical studies on the behavior of RBS connections in moment resisting frames with different types of stiffeners. It was demonstrated that the existence of web stiffeners in IPE beams with reduced sections considerably improves the seismic behavior of these types of connections in moment resisting frames. The static and dynamic behaviors of steel connections with bolted end-plates were experimentally studied by Grimsmo et al. [20]. In both quasi-static and dynamic tests, the failure modes included the failure of the screws along with the plastic deformation of the end-plate.

Using ABAQUS, Rahnavard et al. [21] performed a numerical study on eight connections with different geometries to reduce the area of the flange. Except for the reference sample which produced a high stress in the connection, the other samples had good performances until the drift of 0.06. An innovative technique was introduced by Morrison et al. [22] to augment the seismic performance of connections in moment resisting frames. To undermine the strength of the flange, a thermal operation method was used and the experimental samples were compared with the numerical models. The results revealed that the dimensions of the heated area are suitable provided that they conform to the ones proposed by design codes for RBS connections. Oh et al. [23] evaluated the seismic performance of column-tree moment resisting connections with reduced beam section. By investigating three experimental samples, it was concluded that the details of the RBS can influence the performance of the connection.

The mutual bending–shear effect in short steel beam connections with reduced sections was assessed and analyzed by Crisan and Dubina [24]. Two beam samples with different lengths were experimentally and numerically studied to demonstrate the plastic deformation mechanism of short beams in steel moment resisting frames. The results revealed that the plastic deformations increase as the width to length ratio of the beam increases. In an experimental and numerical study, Tahamouli Roudsari et al. [25] probed the behavior of reduced IPE section with diagonal web stiffeners. By adding diagonal stiffeners to the reduced area, the authors were able to postpone web buckling and significantly increase the ductility of the connection. Investigating multiple experimental and numerical models in that study showed that using diagonal stiffeners stabilizes the hysteresis diagram and also delays its degradation.

Erfani and Akrami [26] studied connections with Reduced Web Sections (RWS). Based on damage indices and by creating elongated circular openings with different dimensions and locations inside the beam's web, they evaluated the failure criteria and energy dissipation. The results showed that with appropriately-sized holes, the RWS connection can significantly improve the seismic behavior of moment resisting frames. Morshedi et al. [27] introduced and evaluated connections with Double Reduced Beam Sections (DRBS). The results showed that the hysteresis behavior of this connection is very suitable and compared to the RBS connection, the deformation capacity of DRBS

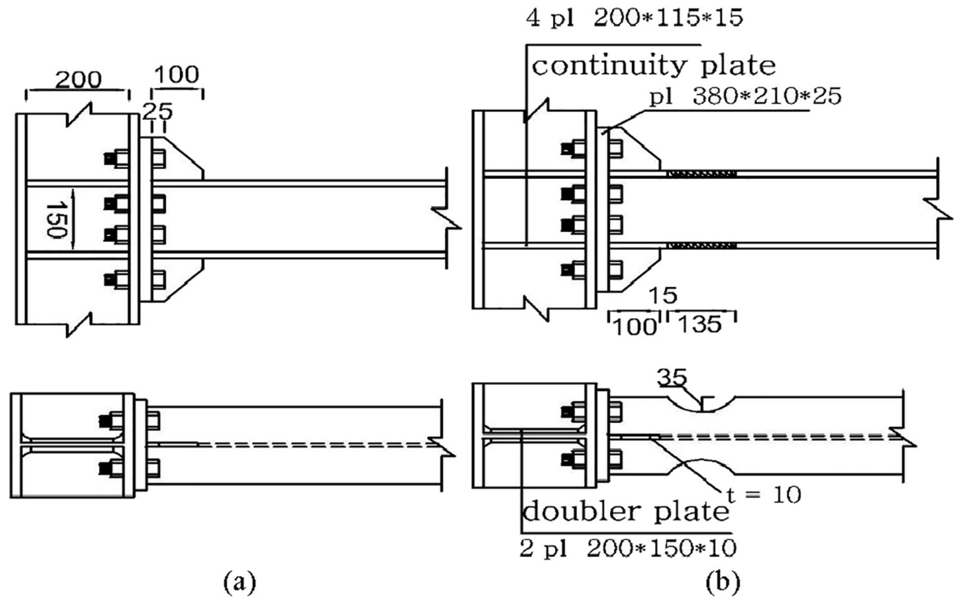

Fig. 1. (a) The OBC sample (b) The RBS sample.

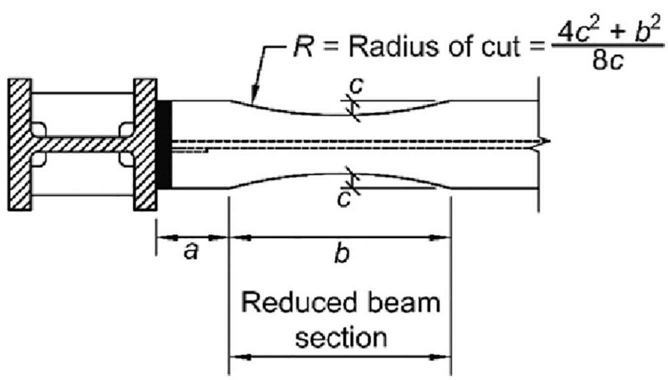

Fig. 2. Details of arched cuts in the beam [1].

connection has increased by 40%. In addition to decreasing stress in the connection, the new detail causes the energy absorption to increase by 50 to 75%.

An experimental and numerical investigation on connections with reduced IPE beam sections incorporating Box-Stiffeners was carried out by Roudsari et al. [28]. Given that reducing the width of the beam's flange in the RBS section potentially increases the probability of lateral torsional buckling, the idea of a Box-Stiffener was proposed to overcome this deficiency. The results revealed that the stiffener considerably increases the ductility of the connection without altering its strength. Montuori and Sagarese [29] made use of steel RBS fuses to increase the ductility of timber structures. They recommended a set of criteria for guaranteeing the creation of the plastic hinge inside the fuse. Ultimately, a design chart was provided which could be used for similar connections.

By creating a plastic hinge outside the connection area, RBS sections minimize the damage inflicted on the panel zone. However, after an

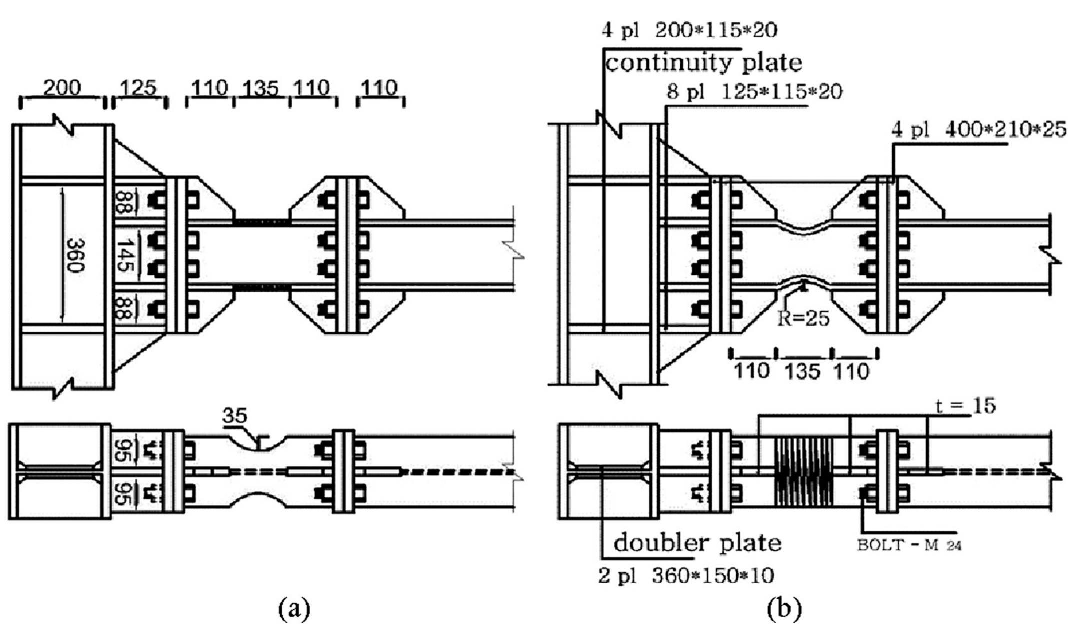

Fig. 3. (a) The RBS-F sample (b) The RDS-F sample.

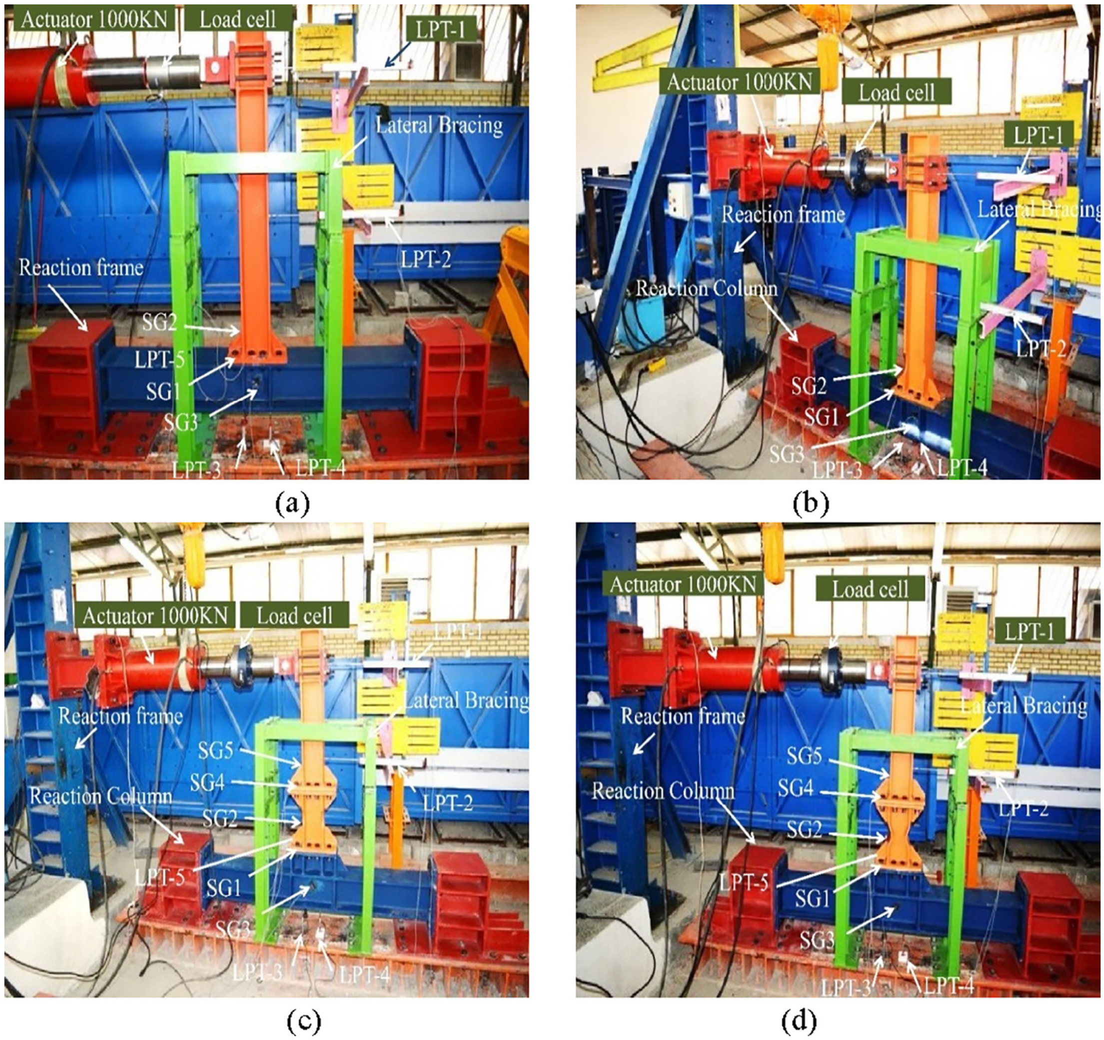

Fig. 4. (a) The OBC sample, (b) The RBS sample, (c) The RBS-F sample, (d) The RDS-F sample.

Table 2
Tensile tests results of the sample.

Plate thickness (mm)	Elasticity modulus (GPa)	Yield stress (MPa)	Ultimate stress (MPa)	Failure strain
25	193.5	329.0	417.7	20.4
20	197.2	355.1	411.9	25.8
15	195.6	350.2	451.0	18.8
10	189.2	268.8	430.1	26.2
8	191.7	240.1	372.1	29.8
Screw	211.1	821.6	1046.6	13.0

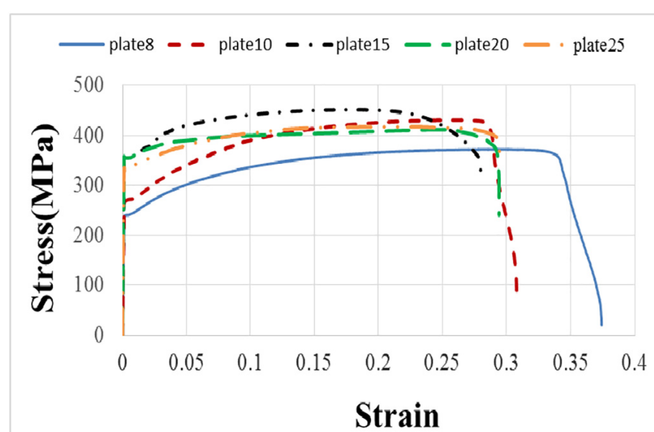

Fig. 5. Stress-strain diagram of all the plates.

average or strong earthquake, the entire beam would have to be replaced due to the concentration of damage in the reduced area, which is almost impossible. The main objective of this experimental study is to investigate the new concept of using the reduced section in a replaceable fuse. To that end, four full-scale experimental samples were constructed and tested. The equivalent European wide flange IPB24 and IPB18 sections were chosen for the column and the beam and the cyclic quasi-static load was applied to the samples until 9% of drift. The first sample was an Ordinary end-plate Bolted Connection with stiffener (OBC) and the second sample was an RBS with end-plate bolted connection and stiffener (RBS).

Under loading, both samples satisfied the special ductility criteria. But, due to the fact that after average or strong earthquakes, damage gets concentrated in the beam and replacing it after the earthquake is either impossible or extremely difficult, a short replaceable fuse was used at the end of the beam in the third and the fourth samples. The third sample incorporated a fuse with the length 35.5 cm and a beam with a reduced flange section (RBS−F). Since the ratio of the flange's width to the beam's height is in direct correlation with the strength of the beam against lateral- torsional buckling, cutting the flange in RBS sections causes different types of buckling to happen faster. To

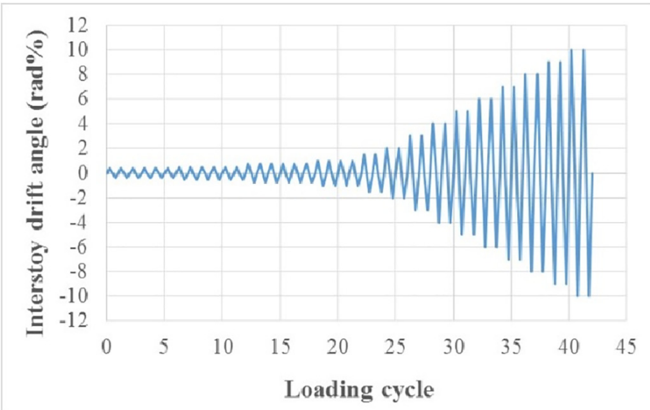

Fig. 6. Loading protocol.

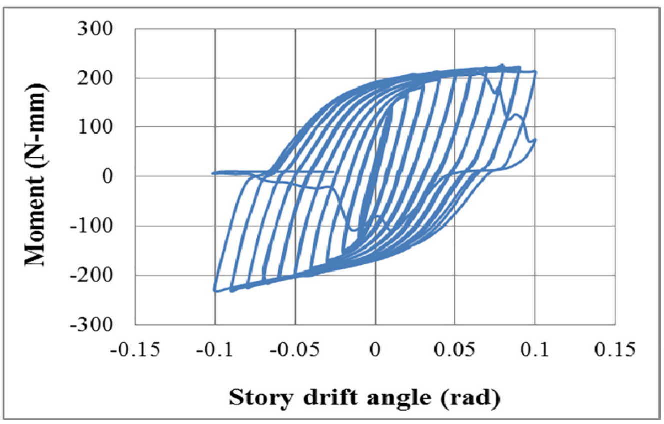

Fig. 7. Moment-drift diagram of the OBC sample.

overcome this problem, in the fourth sample, only the depth of the beam was decreased and the other dimensions remained unchanged. So, the fourth sample also incorporated a 35.5 cm fuse and a beam with reduced depth section (RDS-F).

According to the experimental results, the hysteresis, the backbone, and the equivalent bilinear diagrams of all the samples were drawn and the ductility, energy dissipation, and low cycle fatigue of all the samples were evaluated and compared. The results indicate that the RBS–F and RDS–F samples had better performances compared to the other two connections and both can be used as replaceable fuses in steel moment resisting frames. It is worth mentioning that among the two, the RDS–F sample has a better performance.

2. Test plan

The tests were performed in the structural research lab of the Islamic Azad University of Kermanshah. Four full-scale samples with equivalent IPB sections made of ST37 steel plates were used in the study. For the beam – column bolted end-plate connections, grade 10.9 screws with the diameter of 24 mm were used in accordance with the ISO standard [30].

2.1. Sample specifications and test setup

In all of the four samples, the lengths of the column and the beam (from the centerline of the column to the point where the load is applied) were considered to be 2000 and 1445 mm, respectively. The behavior of the connection is obviously a function of the specifications of the beam, the column, and the panel zone. Since the aim of this study is to assess failure in the beam, the dimensions of the column section and the properties of the panel zone had to be selected so that the overall behavior of the connection would not be affected [31].Thus, to strengthen the panel zone, continuity and doubler plates were used and the section modulus of the column was considered to be two times greater than that of the beam so as to ensure the formation of plastic hinge in the beam. After choosing the beam and column sections based on the strong column-weak beam theory, the details of the connections were designed based on the AISC/ANSI 358–16 standard [1]. This design code is widely employed by researchers to design connections [32,33].The dimensions of the beam and the column, which were seismically compact sections, are given in Table 1.

As it can be seen in Fig. 1, the first sample is an ordinary rigid connection with bolted end-plate and stiffener (OBC). Also, the second sample is a beam with reduced section incorporating bolted end-plate and stiffener (RBS). The dimensions of the reduced area of the flange were selected based on the AISC [1] code, Eq. (1), and Fig. 2. In the third and fourth samples, the reduced section was used in a short replaceable connector which acted as a fuse so as to make the formation of plastic hinge in the component possible (Fig. 3). The end-plate, in conjunction with the screws, furnished the connection of the fuse to the beam and the column. Similar to sample 2, the ordinary reduced flange section was used in sample 3 (RBS−F). In conventional RBS connections, due to the decrease in the flange width to beam height ratio, the possibility of lateral – torsional buckling in the beam increases. In sample four, by changing the geometry of the reduced section, this ratio was increased in order to decrease the possibility of buckling in the beam (Fig. 3). Thus, without changing the dimensions of the beam's flange, the depth of the beam in the fuse was decreased and the fuse with a reduced depth was built (RDS-F).

The height change was carried out so that the beam could have a crescent-like shape which prevents stress concentration. Furthermore, in sample four, the flange in the crescent -like part of the fuse was built using cold rolling which brought about a significant amount of residual stress. In samples three and four, a seating component was placed on the column which acted as a connection between the beam and the column to not only make the probable replacement of the fuse possible, but also to ensure that the column sustains no damage. To prevent the end-plate from separating and also for the reduced section to perform better, a sufficient number of stiffeners were employed in the connection of the beam to the end-plate in all of the samples.

$$\begin{aligned}&0.5b_f \le a \le 0.75b_f\\&0.65d \le b \le 0.85d\\&0.1b_f \le c \le 0.25b_f\end{aligned} \tag{1}$$

To connect the beam/fuses to the end-plate, complete penetrating groove weld was used and for the other items such as connecting the flange to the beam's web, the stiffeners to the beam, the doubler and continuity plates to the column, fillet welding was used. For the weldings, the SMAW process was made use of and the quality of the weldings was controlled using nondestructive testing. To clamp the columns to the strong chassis on the floor of the lab, two supports with the dimensions of 400 × 400 × 500 mm were used. The connection between the support and the chassis was supplied by the end-plates and screws. In the layout of the tests, the column is a horizontal element, connected to the supports through a bolted end-plate connection via eight grade 10.9 screws of diameter 24 mm. Also, as a vertical component, the beam is connected to the column through a bolted end-plate connection by eight grade 10.9 screws with the same grade and diameter. All of the bolted end-plate connections are frictional and were constructed in accordance with the ISO standard [30] and the screws were completely pre-stressed.

Fig. 4 depicts the test setup for all of the four samples. A hydraulic actuator with the minimum capacity of 1000 KN and the displacement capacity of 300 mm in compression and tension was used. To apply the quasi-static cyclic load, one end of the actuator was pinned to the top of the beam and the other end was rigidly fixed to the reaction frame.

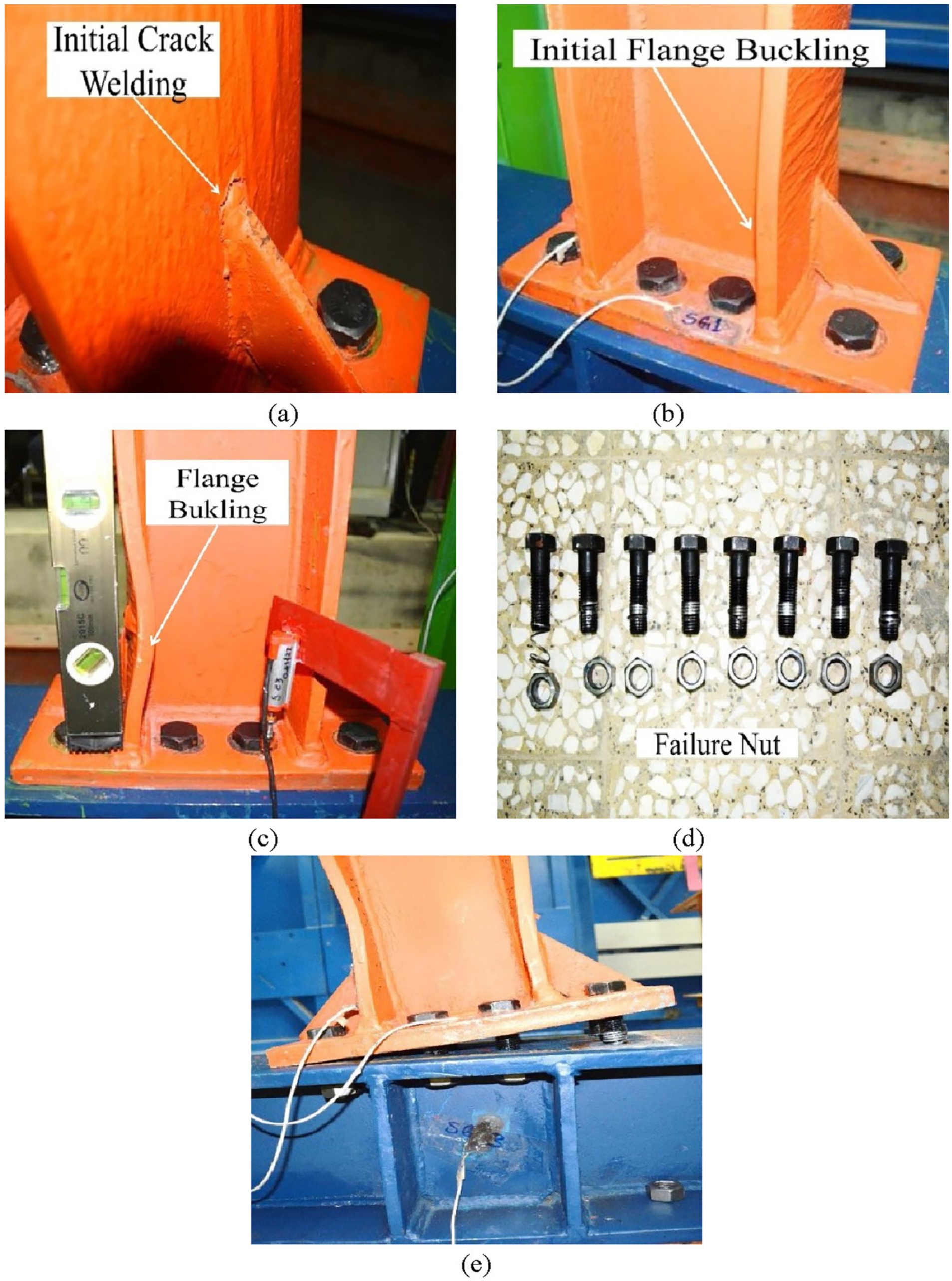

Fig. 8. (a) Initial crack in the welding, (b) initial buckling in the flange of the beam, (c) buckling intensification in the flange of the beam, (d) abrasion of the internal threads of the nut, (e) failure of the connection.

From the top of the end-plate, the elevation of the point the actuator was connected to the beam in the first and second samples was 1300 mm and in the third and the fourth samples, due to the presence of the seating, the elevation was elected to be 1150 mm. For the lateral bracing of the beam, a suitable structure was constructed using the profile IPE160.

To measure the displacement of the end and middle parts of the beam, the rotation of the panel zone, and the separation of the end plate, Linear Potentiometer Transducers (LPTs) with a precision between 0.01 and 0.04 mm were used. Two LPTs with the course length of 450 mm for the end and middle points of the beam, two LPTs with the course length of 50 mm for the panel zone, and to measure the separation of the end plate, two LPTs with the course length of 25 mm were used. In addition, 3 to 5 Strain Gauges (SG) were used in each sample. The installation location of the SGs and the LPTs in the samples are illustrated in Fig. 4. A 32-channel data logger was employed to record the data. To ensure the authenticity of the designed test setup, a series of preliminary Finite Element analyses were performed. These were then used to determine locations of the strain gauges. Also, the results of these analyses revealed that the stroke of the LPTs and the capacity of the load cell were suitable.

2.2. Material properties

For all of the plates used in the beam, the column, the end plates, the stiffeners, and also the screws, tensile tests were carried out in accordance with the ASTM A370 standard [34]. The modulus of elasticity, yield stress, ultimate stress, and failure strain of the materials were obtained. The results are presented in Table 2 and the stress–strain diagrams of all the plates have been drawn and are shown in Fig. 5.

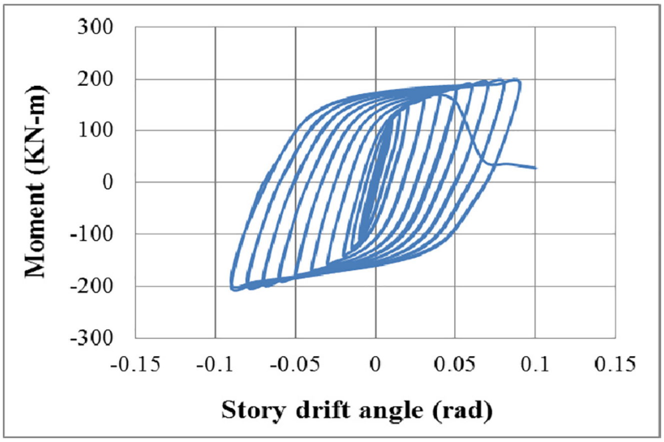

Fig. 9. Moment–drift diagram of the RBS sample.

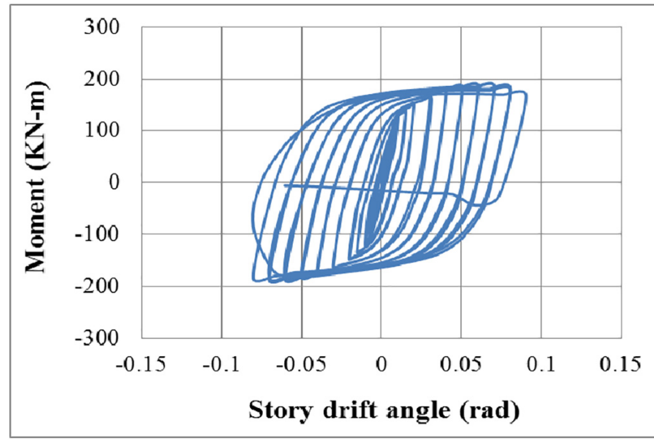

Fig. 11. Moment – drift diagram of the RBS-F sample.

2.3. Loading protocol

For the cyclic loading, the protocol provided in FEMA-350 [35], which is widely used for steel beam-column connections, was employed [11,15,18,20,23,27]; meaning that the drift ratios of 0.00375, 0.005, and 0.0075 were each applied to the beam in six cycles. Then, the drift ratios of 0.01, 0.015, and 0.02 were each applied to the beam in four, two, and two cycles, respectively. Afterwards, in each stage of the two-cycle loadings, 0.01 rad was added and the loading continued to the point of failure in the beam/connection. The loading protocol is illustrated in Fig. 6. The drift values were multiplied by the height of the beam and were applied to the top of it, i.e. 1325 mm from the column's face, as displacements.

3. Test results

All samples were subjected to cyclic loading and their hysteresis moment – drift ratio diagrams were obtained. All four samples satisfied the requirements dictated by AISC [1] regarding special moment resisting frames. The experimental observations including buckling in the flange, buckling in the web, and the type of failure in each of the samples are thoroughly discussed in the following.

3.1. The OBC sample

The hysteresis moment–drift diagram of the OBC sample is depicted in Fig. 7. At a drift of 0.045, the first crack took form in the welding of the connection, between the stiffener and the beam's flange (Fig. 8-a). At 0.054 of drift, the flange of the beam went through local buckling, which can be seen in Fig. 8-b. As it can be seen in Fig. 8–c, at 0.07 of drift, buckling intensifies in the flanges, whereupon the moment–drift diagram starts to experience a slight degradation. The maximum moment in the connection was reached at 220.94 KN-m. Buckling in the beam's web started at a drift lower than 0.08 and continued until the end of loading.

Loading discontinued at 10% of drift, with the nuts separating from the screws (Fig. 8-e and -d). To prevent this, two nuts were used for each screw in the next tests. In any case, the hysteresis diagram is suitable and no pinching effect can be seen. A minor degradation started in the diagram at 7% of drift which was due to buckling intensification in the flange and buckling starting in the web. Until 0.07 of drift, minor cracks initiating in the welding of the stiffeners and the initial buckling of the flange had no effect on the hysteresis diagram. The horizontal slippage that took place at 10% of drift can be attributed to the abrasion and slippage of the internal threads of nut. As it can be seen in Fig. 8, the transition zone in the stiffener on the right side of the OBC sample was not implemented due to a fabrication error. A recent study shows that employing a slope of 45 degrees in rib stiffeners can increase the probability of failure and cracking in weldings [36]. The cracking of the welding at 4.5% of drift highlights the importance of the angle of the stiffeners and the transition zone. However, this minor crack did not significantly expand throughout loading and exerted no influence on the hysteresis diagram of the connection.

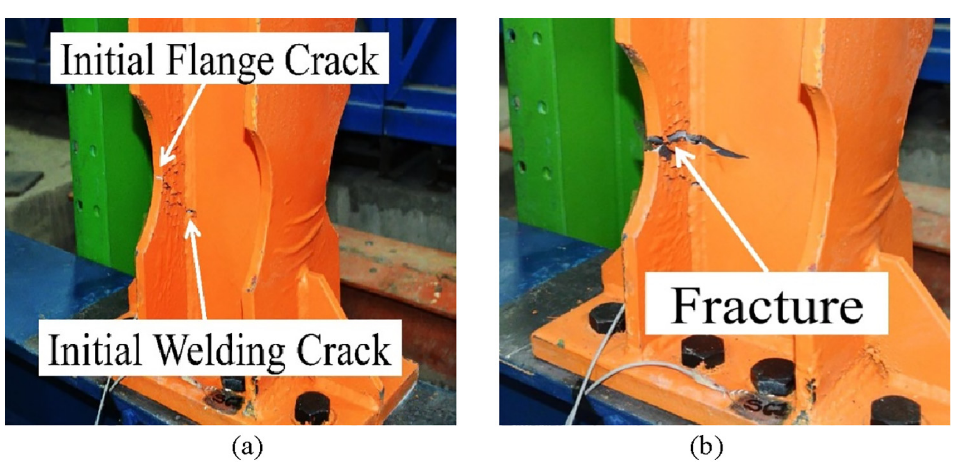

Fig. 10. (a) Crack initiation, (b) failure in the flange and the web of the beam.

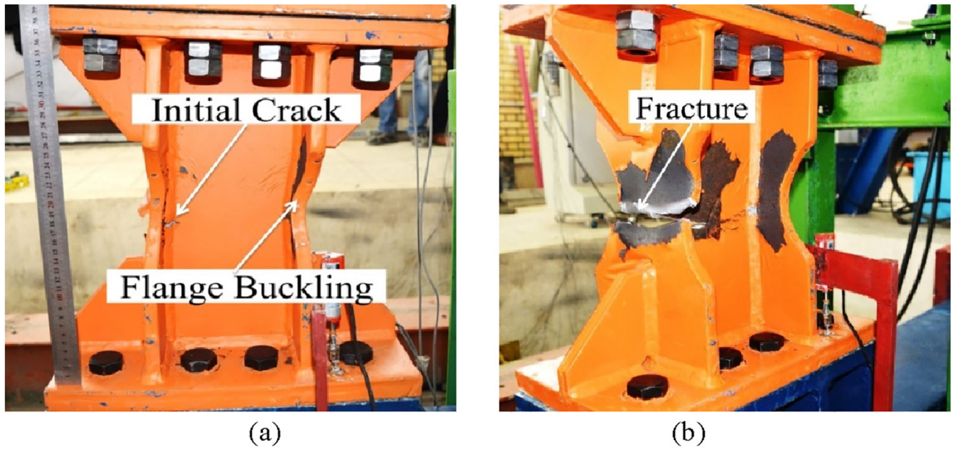

Fig. 12. (a) Buckling and crack initiation in the flange, (b) Failure in the flange and the web of the beam.

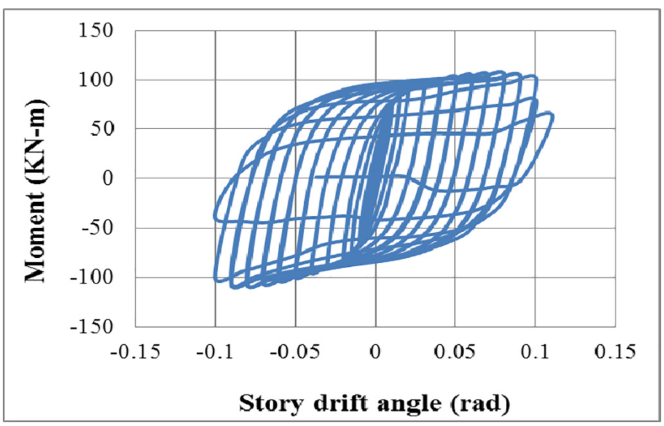

Fig. 13. Moment-drift diagram of the RDS–F sample.

3.2. The RBS sample

The moment–drift diagram of the RBS sample is illustrated in Fig. 9. As a result of the good performance of the connection, nothing noticeable happened to the components of the connection and the beam prior to the drift of 0.08. At 0.08 of drift, the flange went through local buckling in the reduced area and some cracks were observed at the location where the web and the flange meet and also in the middle of the crescent-like area (Fig. 10-a). At a drift of 0.09, the crack in the beam's flange expanded and spread through the web of the beam, thereby causing considerable degradation in the moment–drift diagram and collapse of the connection (Fig. 10–b). The maximum moment in the connection was recorded as 190.54 KN-m, at 0.08 of drift. The performance of the connection is good and no meaningful strength degradation can be seen until the last step of cyclic testing. The act of weakening the beam by reducing its cross section protected the connection from failure and caused damage to be concentrated in the reduced area. Perhaps the only flaw of the connection is that the beam cannot be replaced after a medium-intensity or strong earthquake.

3.3. The RBS-F sample

Fig. 11 displays the moment–drift diagram of the RBS–F sample. Similar exactly to the RBS sample, no significant damage was inflicted on the components of the connection and the beam until 0.07 of drift and the diagram followed an ascending trend. In the second cycle of the 0.07 drift, a slight strength degradation was seen in the diagram which was the result of crack initiation and local buckling in the beam's flange in the reduced area (Fig. 12-a). In the second cycle of the 0.08 drift, with the rapid expansion of the crack and the occurrence of tearing in the flange and a portion of the web, the moment–drift diagram experienced a drastic strength degradation and the connection failed (Fig. 12-b). The maximum moment borne by the connection was equal to 185.16 KN–m, recorded at 0.07 of drift.

From the standpoints of failure type and hysteresis diagram, the performance of the connection was very similar to the RBS sample. The seismic characteristics of the samples will be discussed and compared in the next section, but the advantage of this sample over the RBS sample can be seen in its ability to be replaced.

3.4. The RDS-F sample

As it can be seen in Fig. 13, the moment–drift diagram of the RDS–F sample is very symmetrical and the model has managed to bear a higher drift compared to the other samples. Before the drift of 0.08, no failure occurred in the components of the connection and the beam. In the second cycle of the 0.08 drift, in the location where the web was connected to the flange in the reduced depth section, a crack initiated in the welding and the diagram experienced a nominal strength degradation (Fig. 14-a). As loading continued, at 0.09 of drift and across from the previous crack, the welding connecting the web to the flange cracked and in the second cycle of the same drift, tearing commenced in the web and spread throughout its width (Fig. 14-b). Fig. 14-c shows the crack in the center of the arch of the flange in the first cycle of the 0.10 drift. With loading continuing in the 0.11 drift, the flange in the middle of the arch was completely severed and the connection collapsed (Fig. 14-d). The maximum moment in the connection was recorded at 104.02 KN–m, at the 0.08 drift.

Not only is the connection replaceable after an earthquake, the rotational capacity of the connection is also higher compared to the other samples. Although the RDS-F sample seemed to have a very good performance in terms of stability in the hysteresis diagram, it encountered difficulty in terms of strength. The main reason for this could be found in the connection geometry. Fig. 15 shows the free body diagram of the RDS-F sample. It is clear that the pair of force acting on the flange increased the shear force in the section. Therefore, shear stress in the web was much higher than that of RBS and RBS-F specimens. Fig. 14-b confirms this and shows that the failure of the RDS-F specimen in the laboratory began from the web. A quantitative assessment regarding the bending strength of the RDS-F sample is given at the end of Section 4.1.

4. Discussion and assessment

In this section, the backbone diagram was drawn for all the samples, based upon which the effective stiffness, ductility, yield strength, and

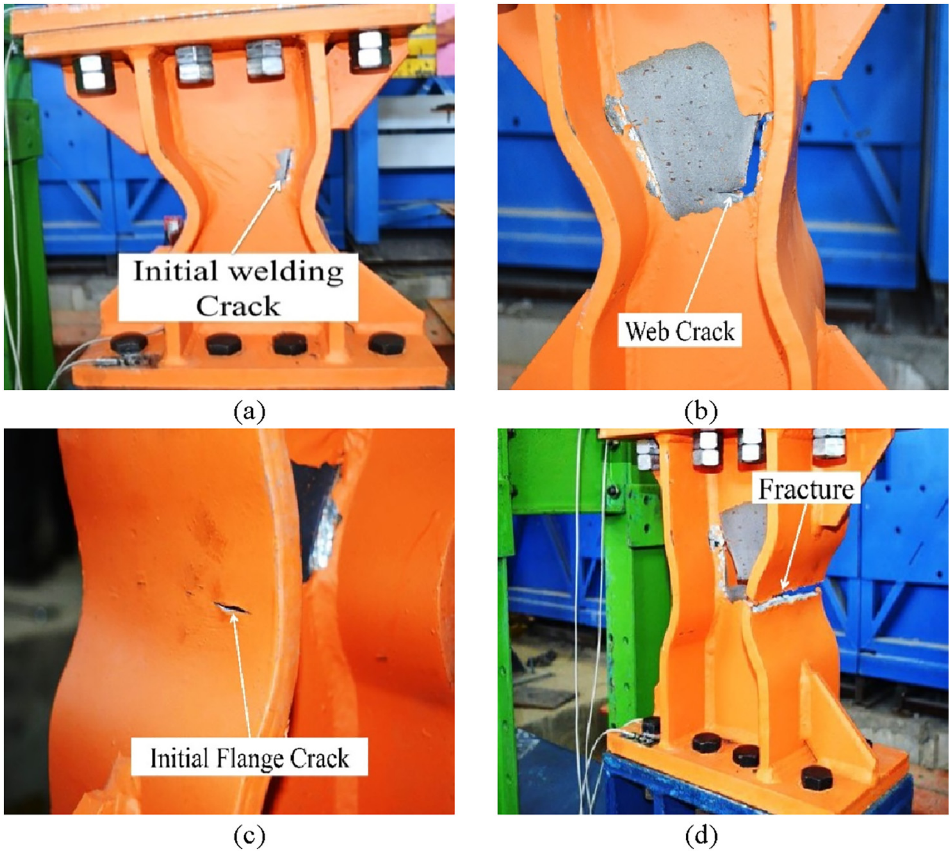

Fig. 14. (a) Crack initiation between the web and the flange, (b) crack in the web, (c) crack initiation in the flange, (d) failure in the flange and the web of the beam.

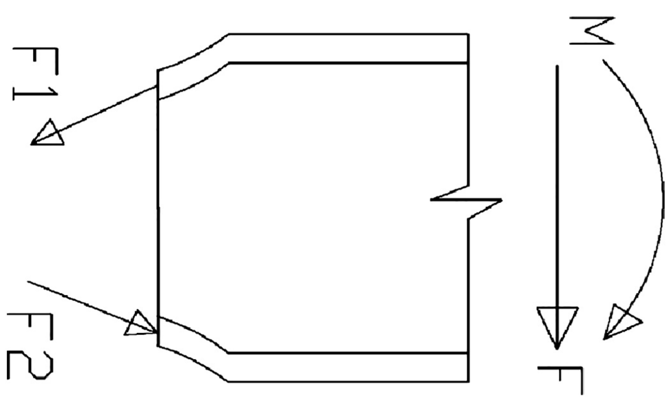

Fig. 15. Free body diagram of the RDS-F sample.

ultimate strength of all the samples were calculated. Also, energy dissipation, strain in the connections, rotation of the panel zone, and low cycle fatigue in the samples were evaluated and compared. By taking into account all the above parameters, a comprehensive comparison can be drawn and the best performance can be selected.

4.1. The backbone and the bilinear diagrams of the samples

In all the four experimental samples, the envelope of the hysteresis moment-drift diagram with the higher strength degradation was the zone for which the backbone diagram was drawn and based on the criteria presented in FEMA–440 [37], the equivalent bilinear diagram was obtained and fitted to the backbone diagram. Only the ascending portion of the hysteresis diagram was used to obtain the backbone diagram and the decreasing segment was overlooked. As it can be observed from Fig. 16, the equivalent bilinear diagram has to be drawn so that the area underneath would be equal to that of the backbone diagram (the concept of equivalent energy) [37]. By drawing the equivalent bilinear diagram, the yield moment (My), yield drift (θy), ultimate moment (Mu), and ultimate drift (θu) were determined and the effective stiffness (Ke) and ductility (μ) can be calculated as follows:

$$\mu = \theta_u/\theta_y \tag{2}$$

$$K_e = M_y/\theta_y \tag{3}$$

Ductility is one of the important parameters in designing a structure which shows the ability of the structure in sustaining deformations that are predominantly in the plastic phase, without any significant strength degradation. The seismic properties of all the four samples are presented in Table 3. From the ductility standpoint, the RBS, RBS-F and RDS-F samples are in better conditions compared to the OBC sample. Also, not only does the RDS-F sample have a higher ductility compared to the RBS sample, it is also much more suitable because of its ability be replaced.

The ultimate strengths of the RBS and RBS–F samples are more or less in the same range. Although the plastic section moduli of these two samples in the weakest section are almost equal, the ultimate strength of the RDS–F sample is much lower than the RBS–F sample. It seems that the reasons behind the reduction in the ultimate strength of the RDS sample are its unique geometry and the diagonal tensile and compressive forces present in the flanges.

For a more accurate assessment, the commercial Finite Element package ABAQUS was used. No damage was seen in the column and the panel zones of the experimental samples. The aim of this section is to investigate the effects of height reduction on the ultimate strength of the RDS sample. So, only one beam with the length of 1150 mm was modeled using the S4R element, i.e. the four-node reduced integration shell element (Fig. 17). This element has six degrees of freedom per node and can take into account material nonlinearity and large

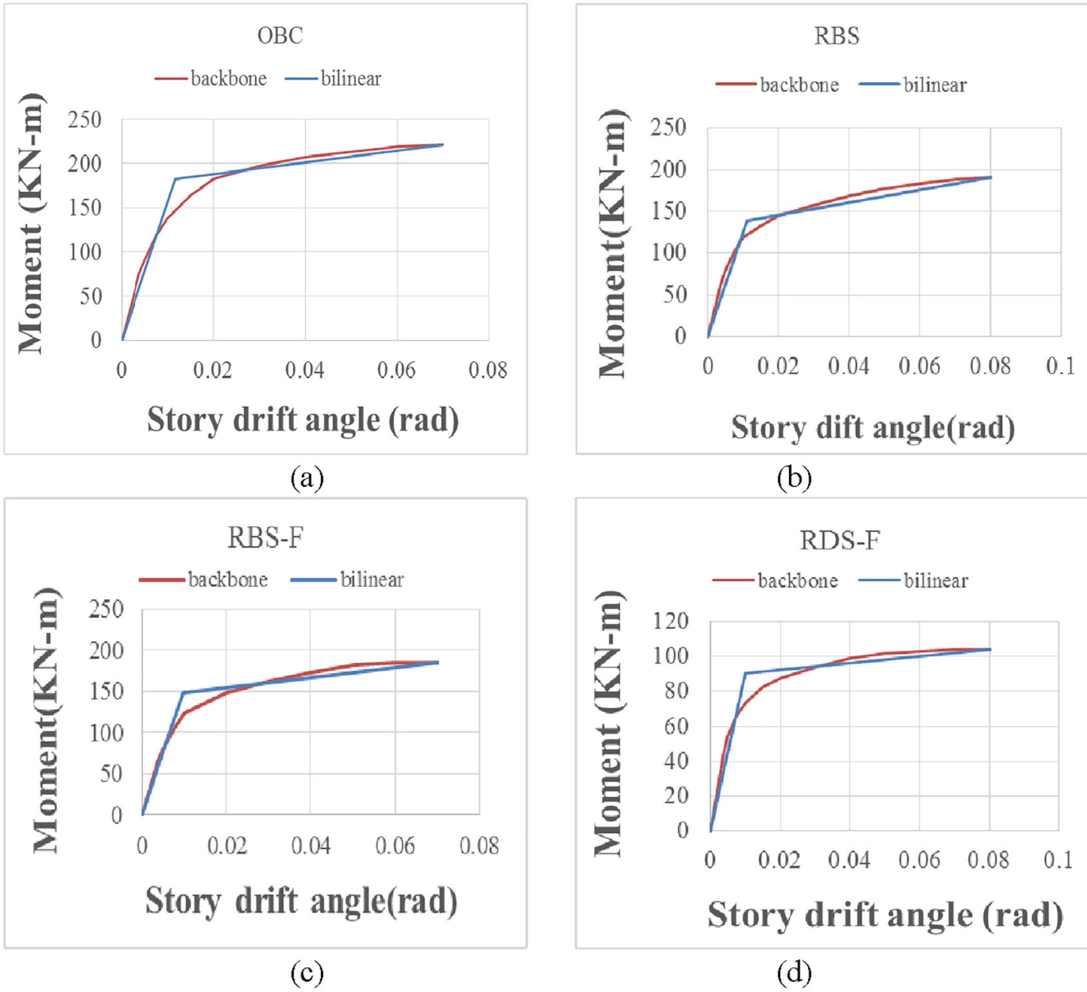

Fig. 16. The backbone and the bilinear diagrams of the samples.

Table 3
The seismic properties of the four samples based on their equivalent bilinear diagrams.

specimen	θ_y %	θ_u%	M_y (KN-m)	M_u (KN-m)	K_e (MN-m)	μ
OBC	1.17	7	182.70	220.94	15.66	5.98
RBS	1.10	8	138.90	190.54	12.63	7.27
RBS-F	0.98	7	148.73	185.16	15.12	7.14
RDS-F	1.02	8	90.63	104.02	8.91	7.84

deformations. The dimensions of the beam's cross-section and its material properties were selected based on Tables 1 and 2, respectively. One end of the beam was considered to be fixed and the other end was pushed over with a displacement equal to 9% of drift. Eight different analyses for the different values of R (R = 0, 5, 10, …, 30, 35 mm) were carried out and the corresponding Mu values were obtained.

Fig. 18 shows the diagram of ultimate bending capacity reduction of the RDS samples with respect to height decrease. In other words, the vertical axis of Fig. 18 represents the ratio of the ultimate moment capacities of the RDS to that of the unreduced section. For the RDS-F sample with R = 25 mm and a strength reduction ratio of 0.47, the ultimate strength was obtained as 0.47 ∗ 220.94 = 103.84 KN which is

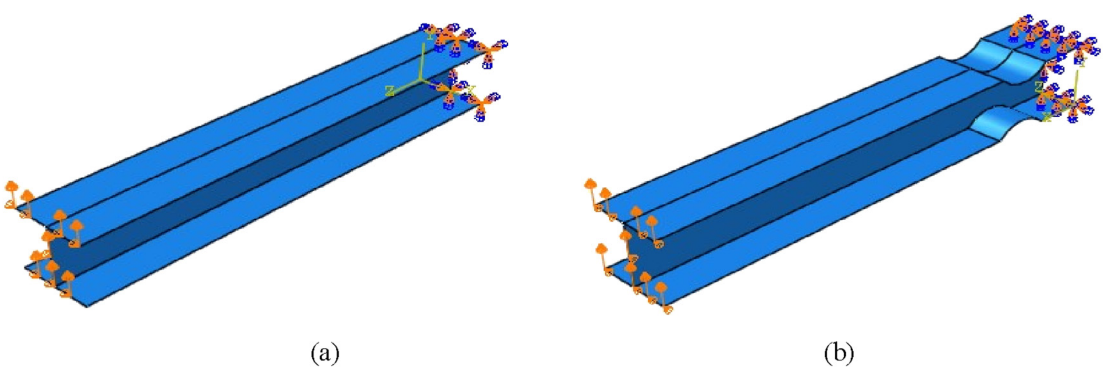

Fig. 17. Numerical model of the RDS sample for a) R = 0 mm and b) R = 30 mm.

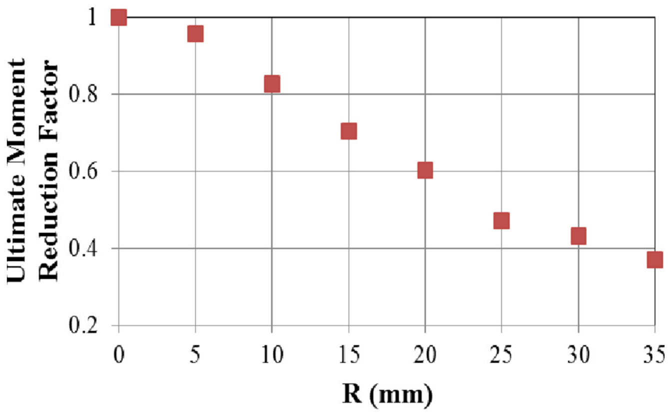

Fig. 18. Ultimate bending capacity reduction against height decrease diagram of the RDS sample.

completely concordant with the experimental results. The interesting thing is that because of the special geometry of the RDS-F sample, it stabilizes the hysteresis diagram, delays buckling, and increases ductility. But, strength degradation in the beam of this sample is quite higher compared to the RBS sample. Thus, special attention must be paid to its strength degradation when the RDS is being used.

The effective stiffness of the RDS–F sample is lower than the rest of the samples which can be ascribed to the decrease in the ultimate strength. As the results in Table 3 show, the effective stiffness of the RBS–F sample is somewhat higher than the RBS sample. Therefore, using the fuse would increase the rigidity of the beam and subsequently the lateral stiffness of the frame. This stiffness increase has a positive effect in the overall performance of the frame.

Table 4
Comparing the maximum absolute values of strain in the samples.

	SG1	SG2	SG3
OBC	0.00370	0.01166	0.00035
RBS	0.00064	0.00459	0.00022
RBS-F	0.00109	0.01407	0.00027
RDS-F	0.00070	0.006638	0.00021

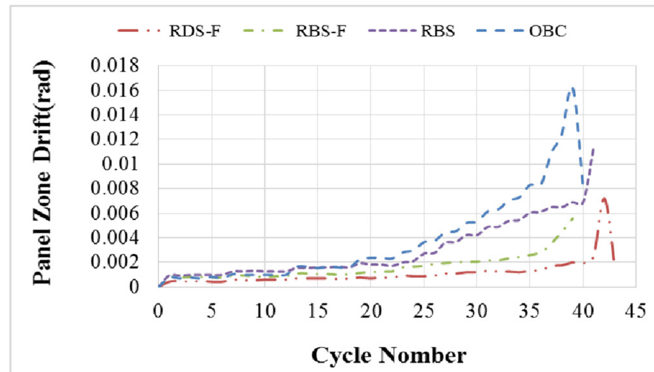

Fig. 20. Comparing the rotation of the panel zone in the samples.

4.2. Strain gauge outputs and rotation in the panel zone

In Fig. 19, the maximum absolute strain in the samples in each cycle throughout loading are shown. In all of the samples, strain in SG2 and SG3, which were placed respectively on the flange of the beam and in the panel zone, recorded the highest and the lowest values, respectively. Table 4 compares the maximum strains in strain gauges 1, 2, and

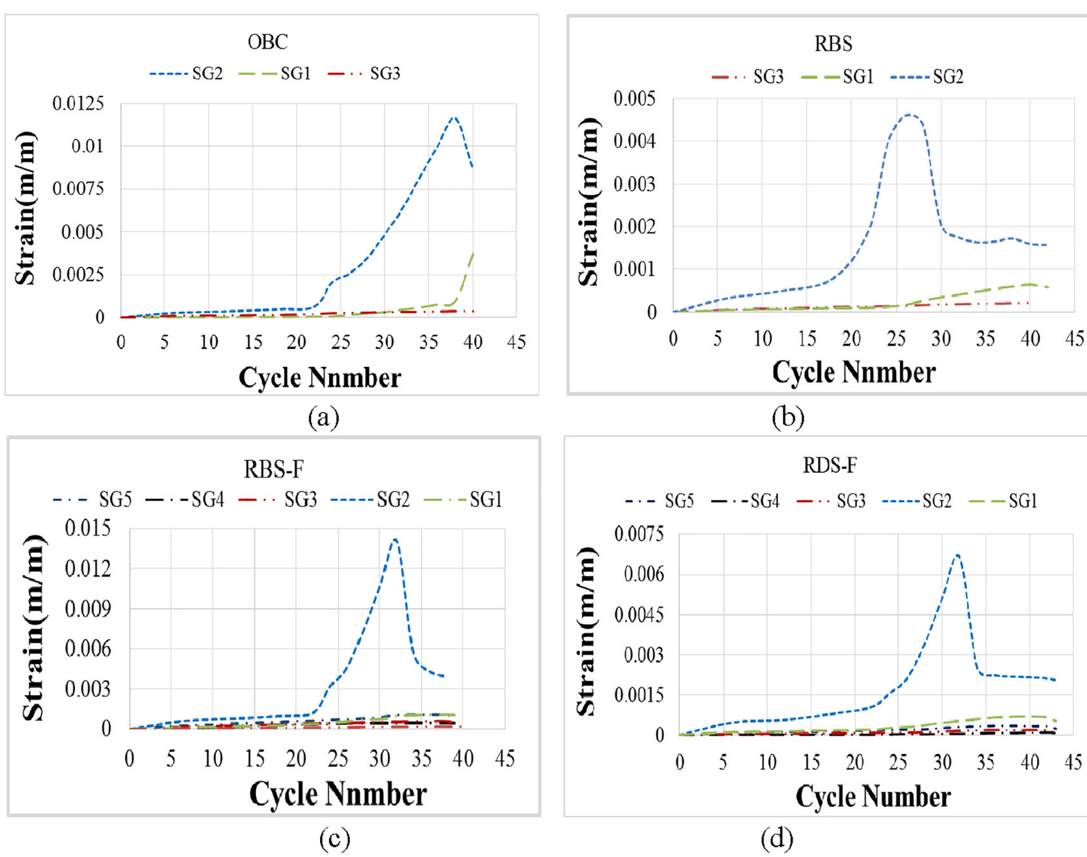

Fig. 19. Strain change diagram in the strain gauges.

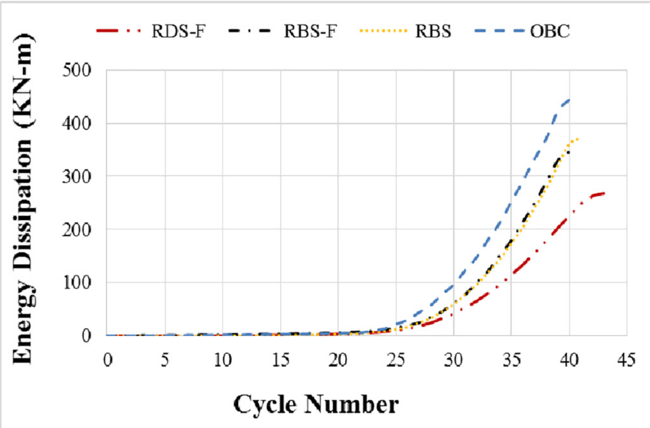

Fig. 21. Cumulative energy dissipation diagram in the samples.

Table 5
The maximum cumulative energy dissipation to M_u ratio of the four samples.

OBC	RBS	RBS-F	RDS-F
2.01	1.95	1.88	2.58

3 for all the four samples. Strain in SG1 in the OBC sample is 3 to 6 times higher than the other samples. Also, strain in SG3 in the OBC sample is 30 to 70% higher compared to the other samples. These results show the capability of the RBS or the RDS samples in protecting and expelling damage from the end-plate and the panel zone.

The rotation of the panel zone can be calculated based on the results from LPT3 and LPT4. Fig. 20 shows the maximum absolute rotation of the panel zone throughout loading in the samples. The highest rotation is related to the OBC sample followed by the RBS sample. Further, the lowest rotation is related to the RBS-F and RDS-F samples. So, these two replaceable samples also provide the highest protection for the panel zone.

4.3. Energy dissipation

Energy dissipation is one of the important seismic characteristics of any connection under cyclic load and is calculated based on the area under the moment–rotation diagram in each cycle. Fig. 21 shows the cumulative energy dissipation of the samples. It is clear that the OBC sample has the highest energy dissipation. One of the reasons behind that is the higher ultimate strength in this connection. The ratio of the maximum cumulative energy dissipation to the M_u of the four samples

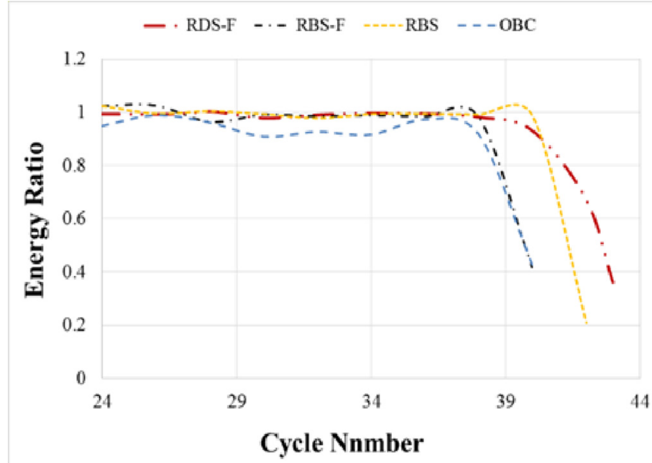

Fig. 23. Low cycle fatigue effect throughout loading.

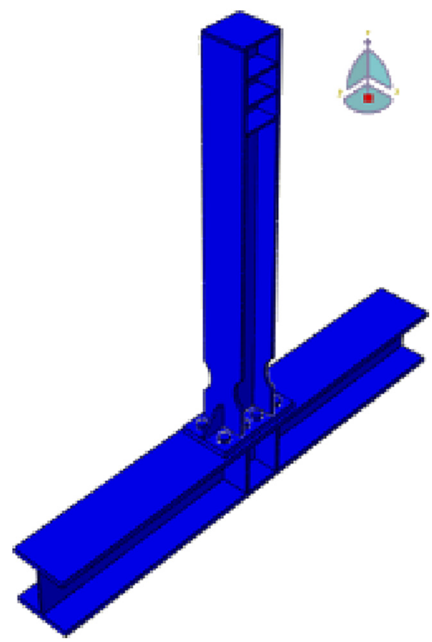

Fig. 24. Finite Element model of the RBS sample.

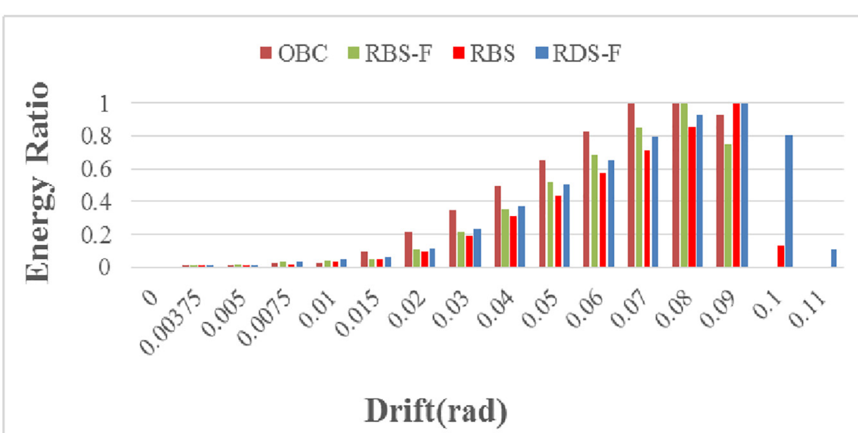

Fig. 22. The normalized energy dissipation diagram.

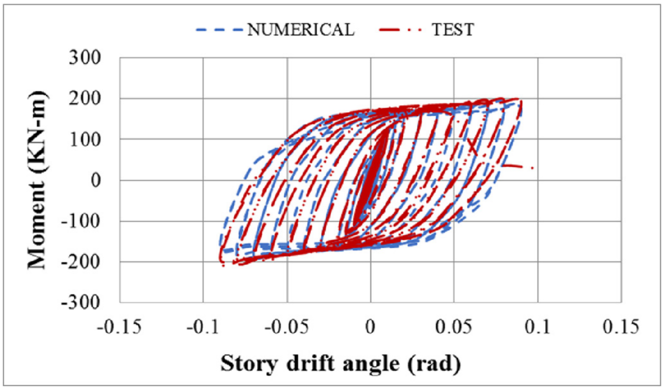

Fig. 25. Comparison between the numerical and experimental hysteresis diagrams of the RBS sample.

Table 6
Maximum values of shear and moment obtained from the 10 Finite Element analyses with respect to the beam's length.

L(mm)	V(KN)	M(KN-m)	V/V_{max}	M/M_{max}
500	219.4	109.7	1.00	0.57
700	216.3	151.4	0.99	0.79
900	196.8	177.1	0.90	0.92
1100	172.7	190.0	0.79	0.99
1300	147.1	191.2	0.67	1.00
1500	127.5	191.3	0.58	1.00
1700	112.5	191.2	0.51	1.00
1900	100.8	191.5	0.46	1.00
2100	91.2	191.5	0.42	1.00
3000	63.9	191.6	0.29	1.00
	V_{max} = 219.4	M_{max} = 191.6		

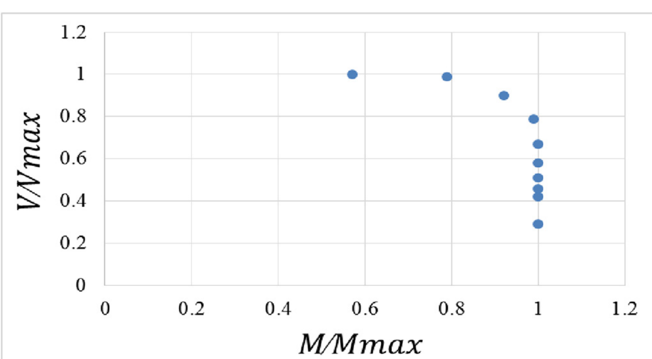

Fig. 26. M/V capacity ratio in the RBS sample.

are given in Table 5. The highest ratio corresponds to the RDS–F sample. For the other samples, however, the results are in the same range.

Fig. 22 demonstrates the normalized energy dissipation diagram of the samples throughout loading. To normalize the diagrams, the energy dissipation in all of the cycles of each sample was obtained and the entire values were divided by the maximum cyclic energy dissipation of each sample. The increase of energy dissipation of the RBS-F and RBS samples continued until the drift of 0.09. For the RDS-F sample, energy dissipation is significant even at a drift of 0.1. From this view point, these three samples have performed desirably.

4.4. Assessing the low cycle fatigue in the samples

Fig. 23 shows the low cycle fatigue effect in each of the four samples throughout loading. It is evident that the strength degradation in the samples due to repetitive loading is very small and the results of all the four samples are suitable. It has to be mentioned that the most stable diagram and the lowest degradation belong to the RDS– F sample.

5. Evaluating the effect of moment to shear ratio (M/V) in the experimental samples

In the tested samples, beams with limited lengths were used. The bending to shear capacity ratio of the beam is a function of the beam's length. If the aim is to evaluate the bending capacity of the beam and the manner in which plastic hinge forms, the length of the beam has to be considered long enough so that only a small percentage of the beam's capacity gets allocated to the shear force. In this section, after verifying experimental results of the RBS sample via Finite Element modeling, the effect of the beam's length on its bending to shear (M/V) capacity ratio will be investigated so that the authenticity of the experimental results can be ensured.

5.1. Finite element modeling and verification

In this section, based on the material properties obtained through tensile testing (Table 2 and Fig. 5), the numerical model of the RBS sample was constructed in ABAQUS. The numerical analysis was carried out with the geometrical and material nonlinearities having been considered. The C3D8R element, an 8-node reduced integration solid element was used in the modeling procedure. The support and loading conditions in the numerical models were considered identical to the experimental sample. The Finite Element model of the RBS sample is shown in Fig. 24. In the locations where surfaces made contact (such as the surfaces between the end plates and the column, the bolt heads and the end plates, the body of the bolt and the inner surface of the hole, and the nut and the columns flange), "Hard Contact" and "Friction" were respectively used along the vertical and horizontal directions [38–41]. Given that until the last step of cyclic loading in the RBS sample no substantial failure took place in the weldings, they were not considered in the numerical model. In other words, the connection of the rib stiffener to the beam and the end plate was modeled using the "Tie" constraint. The Von Mises yield criterion, in conjunction with the "Combined Plastic Hardening Model", were used for the yielding of the material. A displacement-control load was applied to the sample and the static general/standard analysis in ABAQUS was employed in the FE analyses.

In the numerical models, the screws were pre-stressed in the first step. Then, in the second step, lateral cyclic loading was applied to the end of the beam, exactly in accordance with the experimental sample. A comparison between the numerical and experimental results is given in Fig. 25. There is a very good agreement between the numerical and experimental results which can be used to assess the effect of the beam's length on its (M/V) capacity ratio. The minor discrepancy between the results of the numerical and experimental models could stem from the residual stress in the weldings or the geometric imperfection that were not accounted for in the numerical model.

5.2. Investigating the M/V ratio

To investigate the M/V ratio, 10 numerical models of the RBS sample were constructed. In these models, the sole varying parameter is the length of the beam, varying between 500 mm to 3000 mm. The location upon which the lateral load was applied was the same as in the experiment, but uniform loading (Push-over) was employed. From the analysis of each of the numerical models, the values of maximum shear (V) and moment (M) were calculated. Table 6 and Fig. 26 show the values of maximum shear and moment for the 10 numerical models.

The results show that beams with the length of 1100 mm or higher reach up to > 99% percent of their bending capacities. Therefore, it is justifiable to use beams of length 1300 mm in the experimental samples. In addition, according to the AISC-358-16 standard, the ratio of the beam's free span to its depth in RBS connections in special moment resisting frame should not be < 7. In the deformation of a moment resisting frame subjected to lateral loading, moment is almost nonexistent in the mid-span of the beam. Therefore, for experimental studies, many researchers separate the beam from the zero-moment location. In other words, if the length of the beam in the experimental sample is equal to L, the actual length of the beam in an actual frame would be 2 L. Thereupon, the length to depth ratio of the beam of the RBS sample in this study was considered to be $2 \times 1300/180 = 14.4$, which is far larger than 7.

6. Conclusion

In RBS connections, due to damage concentration in the reduced area, the entire beam needs to be replaced after an average or strong earthquake, which in practice is not possible. In this paper, based on experimental tests, the possibility of using the reduced section in a replaceable fuse was probed. To that end, four full-scale specimens including an ordinary bolted end-plate rigid connection (OBC), a reduced beam section and bolted end-plate (RBS), a sample with fuse and reduced flange section (RBS−F), and one with fuse and reduced depth section (RDS-F) were constructed. Cyclic quasi-static load was applied until the drift of 9% and the following results were acquired:

- Compared to the OBC sample, the performances of the three samples with reduced sections in many instances were much better. For instance, damage initiation in the OBC sample took place at 0.045 of drift, whereas in the other samples, damage started at the drift of 0.07. In the OBC sample, the maximum strain was 3 to 6 times in the end plate and 1.3 to 1.7 times in the panel zone higher than the other samples. Therefore, the samples with a reduced section provide a better protection for the panel zone and the column.
- One of the major advantages of the RBS–F and RDS–F samples over the other two samples is their replaceability. In addition to that, these two samples had a significant amount of ductility and a lower rotation in the panel zone, which complement their positive performances.
- In most aspects, the performance of the RDS–F sample was better than the RBS–F sample, among which higher ductility, higher energy dissipation with respect to ultimate strength of the section, and weaker effects of low cycle fatigue can be named.

The main problem with the RDS-F sample is the high reduction in the bending strength of the beam. Although using the rolled RDS section reduces residual stress and improves performance, it does not increase the ultimate strength of the section. One suitable solution is to use steels with higher yield stress in the RDS fuse zone. It has to be noted that in most cases, steels with higher yield stresses cause ductility to decrease, which would render their use in the reduced section irrational. Therefore, it is necessary to use steels with higher yield stress and high ductility. In this case, using the RDS-F sample would be the best choice and it is highly recommended for it to be used in areas with high relative seismic risk. Otherwise, the RBS-F sample is a good replacement for the RDS-F sample. If the fuse-incorporated moment resisting frame is designed correctly, the first area prone to sustaining any damage would be the fuse itself. In this case, the replaceability of the fuses would make the rehabilitation process of structures very convenient. But, fuse replacement is possible only if the columns and the entire structure have not sustained any kind of severe damage. Also, it has to be mentioned that the fuse can only be replaced at small drifts (about 0.01) and after that, due to the increased probability of twisting, the replacement would be difficult. Therefore, more research needs to be carried out regarding the replacement possibility of RBS and RDS fuses after the occurrence of an earthquake. The results of the Finite Element analyses of M/V capacity ratio of the RBS sample showed that the beam's length in the experimental sample is suitable and the sample has reached its maximum bending capacity.

The recent study was done on a wide–flange beam, with a specific level of cross-section reduction, without taking into account the vertical load. To expand the scope of the present study, further research could be done on assessing the effects of different levels of section reduction and also including the influence of vertical load. Also, change in the specifications of the column, the panel zone, and the doubler/continuity plates can drastically influence the behavior of the connection. Although in this research the dimensions were selected so as to concentrate the entirety of the damage on the reduced zone of the beam, additional investigations have to be carried out regarding the use of RBS–F and RDS–F in partially restrained moment connections.

Acknowledgment

The authors would like to gratefully thank the structural research lab of the Islamic Azad University of Kermanshah and the 'NOVIN SAZE FIDER ZAGROSS' company.

References

[1] American Institute of Steel Construction (ANSI/AISC 358–16). Prequalified connections for special and intermediate steel moment frames for seismic applications Chicago, Illinois 2016.
[2] Tremblay R, Filiatrault A, Timler P, Bruneau M. Performance of steel structures during the 1994 Northridge earthquake. Can J Civ Eng 1995;22(2):338–60.
[3] Tremblay R, Filiatrault A, Bruneau M, Nakashima M, Prion HG, DeVall R. Seismic design of steel buildings: lessons from the 1995 Hyogo-ken Nanbu earthquake. Can J Civ Eng 1996;23(3):727–56.
[4] Zhang Xiaofeng, Ricles James M. Experimental evaluation of reduced beam section connections to deep columns. J Struct Eng 2006;132(3):346–57.
[5] Wilkinson Sean, Hurdman Gordon, Crowther Adrian. A moment resisting connection for earthquake resistant structures. J Constr Steel Res 2006;62(3):295–302.
[6] Han Sang-Whan, Moon Ki-Hoon, Stojadinovic Bozidar. Design equations for moment strength of RBS-B connections. J Constr Steel Res 2009;65(5):1087–95.
[7] Hedayat AA, Celikag M. Post-Northridge connection with modified beam end configuration to enhance strength and ductility. J Constr Steel Res 2009;65(7):1413–30.
[8] Pachoumis DT, Galoussis EG, Kalfas CN, Christitsas AD. Reduced beam section moment connections subjected to cyclic loading: experimental analysis and FEM simulation. Eng Struct 2009;31(1):216–23.
[9] Mirghaderi Seyed Rasoul, Torabian Shahabeddin, Imanpour Ali. Seismic performance of the accordion-web RBS connection. J Constr Steel Res 2010;66(2):277–88.
[10] Shen Yunlu, Christopoulos Constantin, Mansour Nabil, Tremblay Robert. Seismic design and performance of steel moment-resisting frames with nonlinear replaceable links. J Struct Eng 2010;137:1107–17.
[11] Mashaly Elsayed, El-Heweity Mohamed, Abou-Elfath Hamdy, Osman Mohamed. Behavior of four-bolt extended end-plate connection subjected to lateral loading. Alex Eng J 2011;50(1):79–90.
[12] Chi Jia Xiang, Nie Shao Feng, Zhou Tian Hua, Sun Tao. Research on seismic behavior of concrete filled square tubular joints with reduced beam section under cyclic loading. Adv Mat Res 2011;243:885–8.
[13] Maleki Shervin, Tabbakhha Maryam. Numerical study of slotted-web–reduced-flange moment connection. J Constr Steel Res 2012;69(1):1–7.
[14] Ghassemieh M, Kiani J. Seismic evaluation of reduced beam section frames considering connection flexibility. Struct Design Tall Spec Build 2013;22(16):1248–69.
[15] Montuori R. The influence of gravity loads on the seismic design of RBS connections. Open Constr Build Technol J 2014;8(1):248–61.
[16] Sofias CE, Kalfas CN, Pachoumis DT. Experimental and FEM analysis of reduced beam section moment endplate connections under cyclic loading. Eng Struct 2014;59:320–9.
[17] Swati Ajay Kulkarni, Gaurang Vesmawala. Study of steel moment connection with and without reduced beam section. Case Stud Struct Eng 2014;1:26–31.
[18] Abdollahzadeh Gholamreza, Hashemi Seyed, Tavakoli Hamidreza, Rahami Hosein. Determination of hysteretic behavior of steel end-plate beam-to-column connection with mechanical and neural network modeling. Arab J Sci Eng 2014;39(11):7661–71.
[19] Roudsari M, Tahamouli F, Abdollahi H, Salimi S Azizi, Khosravi AR. The effect of stiffener on behavior of reduced beam section connections in steel moment-resisting frames. Int J Steel Struct 2015;15(4):827–34.
[20] Grimsmo EL, Clausen AH, Langseth M, Aalberg A. An experimental study of static and dynamic behaviour of bolted end-plate joints of steel. Int J Impact Eng 2015;85:132–45.
[21] Rahnavard R, Hassanipour A, Siahpolo N. Analytical study on new types of reduced beam section moment connections affecting cyclic behavior. Case Stud Struct Eng 2015;3:33–51.
[22] Morrison Machel, Schweizer Doug, Hassan Tasnim. An innovative seismic performance enhancement technique for steel building moment resisting connections. J

Constr Steel Res 2015;109:34–46.
[23] Oh K, Lee K, Chen L, Hong SB, Yang Y. Seismic performance evaluation of weak axis column-tree moment connections with reduced beam section. J Constr Steel Res 2015;105:28–38.
[24] Crisan Andrei, Dubina Dan. Bending–shear interaction in short coupling steel beams with reduced beam section. J Constr Steel Res 2016;122:190–7.
[25] Tahamouli Roudsari M, Jamshidi K. H, Mohebi Zangeneh M. Experimental and numerical investigation of IPE reduced beam sections with diagonal web stiffeners. J Earthq Eng 2016:1–20.
[26] Erfani Saeed, Akrami Vahid. Increasing seismic energy dissipation of steel moment frames using reduced web section (RWS) connection. J Earthq Eng 2017;21(7):1090–112.
[27] Morshedi Mohamad A, Dolatshahi Kiarash M, Maleki Shervin. Double reduced beam section connection. J Constr Steel Res 2017;138:283–97.
[28] Roudsari M Tahamouli, Jamshidi H, Moradi SH. Experimental and numerical assessment of reduced IPE beam sections connections with box-stiffener. Int J Steel Struct 2018;18(1):255–63.
[29] Montuori R, Sagarese V. The use of steel rbs to increase ductility of wooden beams. Eng Struct 2018;169:154–61.
[30] International Organization for Standardization (ISO). ISO 898-1. Mechanical properties of fasteners made of carbon steel and alloy steel —Part 1: bolts, screws and studs with pacified property classes — coarse thread and fine pitch thread Geneva, Switzerland 2009.
[31] Lee CH, Sang-Woo J, Jin-Ho K, Chia-Ming U. Effects of panel zone strength and beam web connection method on seismic performance of reduced beam section steel moment connections. J Struct Eng 2005;131(12):1854–65.
[32] D'Aniello M, Tartaglia R, Costanzo S, Landolfo R. Seismic design of extended stiffened end-plate joints in the framework of Eurocodes. J Constr Steel Res 2017;128P:512–27.
[33] Tartaglia R, D'Aniello M, Rassati GA, Swanson JA, Landolfo R. Full strength extended stiffened end-plate joints: AISC vs recent European design criteria. Eng Struct 2018;159:155–71.
[34] American Society for Testing and Materials (ASTM). Standard test methods and definitions for mechanical testing of steel products. ASTM Standard A370-02 2002. Philadelphia, PA.
[35] FEMA. Recommended seismic design provisions for new moment frame buildings report. FEMA 350 Washington DC: Federal Emergency Management Agency; 2000.
[36] Tartaglia R, D'Aniello M, Landolfo R. The influence of rib stiffeners on the response of extended end-plate joints. J Constr Steel Res 2018;148:669–90.
[37] FEMA. Improvement of nonlinear static seismic analysis procedures. FEMA-440 Redwood City: Federal Emergency Management Agency; 2005.
[38] Tartaglia R, D'Aniello M, Zimbru M, Landolfo R. Finite element simulations on the ultimate response of extended stiffened end-plate joints. Steel Compos Struct 2018;27(6):727–45.
[39] Brunesi E, Nascimbene R, Rassati GA. Seismic response of MRFs with partially-restrained bolted beam-to-column connections through FE analyses. J Constr Steel Res 2015;107:37–49.
[40] Brunesi E, Nascimbene R, Rassati GA. Response of partially-restrained bolted beam-to-column connections under cyclic loads. J Constr Steel Res 2014;97:24–38.
[41] Coelho AMG. Rotation capacity of partial strength steel joints with three-dimensional finite element approach. Comput Struct 2013;116:88–97.